Intrinsic regulation of FIC-domain AMP-transferases by oligomerization and automodification

Frédéric V. Stanger[a,b], Björn M. Burmann[a], Alexander Harms[b], Hugo Aragão[a], Adam Mazur[c], Timothy Sharpe[d], Christoph Dehio[b,1], Sebastian Hiller[a,1], and Tilman Schirmer[a,1]

[a]Focal Area Structural Biology and Biophysics, Biozentrum, University of Basel, CH-4056 Basel, Switzerland; [b]Focal Area Infection Biology, Biozentrum, University of Basel, CH-4056 Basel, Switzerland; [c]Research IT, Biozentrum, University of Basel, CH-4056 Basel, Switzerland; and [d]Biophysics Facility, Biozentrum, University of Basel, CH-4056 Basel, Switzerland

Edited by Anthony Maxwell, John Innes Centre, Norwich, United Kingdom, and accepted by the Editorial Board December 15, 2015 (received for review August 27, 2015)

Filamentation induced by cyclic AMP (FIC)-domain enzymes catalyze adenylylation or other posttranslational modifications of target proteins to control their function. Recently, we have shown that Fic enzymes are autoinhibited by an α-helix (α_{inh}) that partly obstructs the active site. For the single-domain class III Fic proteins, the α_{inh} is located at the C terminus and its deletion relieves autoinhibition. However, it has remained unclear how activation occurs naturally. Here, we show by structural, biophysical, and enzymatic analyses combined with in vivo data that the class III Fic protein NmFic from *Neisseria meningitidis* gets autoadenylylated *in cis*, thereby autonomously relieving autoinhibition and thus allowing subsequent adenylylation of its target, the DNA gyrase subunit GyrB. Furthermore, we show that NmFic activation is antagonized by tetramerization. The combination of autoadenylylation and tetramerization results in nonmonotonic concentration dependence of NmFic activity and a pronounced lag phase in the progress of target adenylylation. Bioinformatic analyses indicate that this elaborate dual-control mechanism is conserved throughout class III Fic proteins.

adenylylation | AMPylation | posttranslational modification | enzyme regulation | molecular timer

Fic (filamentation induced by cyclic AMP) proteins containing the FIC domain (pfam 02661) are found in all kingdoms of life. FIC domains encode enzymatic activities that modulate target protein function by diverse posttranslational modifications (1, 2). The vast majority of known Fic proteins are AMP-transferases that use ATP to catalyze the transfer of an AMP moiety onto a target hydroxyl side chain (3, 4). This reaction is akin to the situation in protein kinases, which catalyze γ-phosphate transfer onto target side chains.

Only a few Fic targets have been identified to date (2). IbpA (4) and VopS (3), two bacterial FIC-domain effectors that get translocated into host cells, catalyze the adenylylation of Rho GTPases, resulting in cytoskeleton collapse. Most recently, we have found that a subset of bacterial Fic proteins adenylylates DNA gyrase and topoisomerase IV, which leads to their inactivation and cellular growth arrest (5). The structure of a FIC-domain/target complex (6) and the catalytic mechanism have been determined (6, 7). However, the biological functions, as well as the molecular mechanism, of the vast majority of Fic proteins have remained elusive. Intriguingly, in vitro automodification has been demonstrated for most Fic proteins that have been described so far (6, 8–15), but its physiological relevance has remained unclear.

Recently, we have shown that Fic-mediated adenylylation is tightly regulated (8). In the native state, a helix partly obstructs the ATP binding site with a strictly conserved Glu blocking ATP γ-phosphate binding, thereby preventing productive/competent substrate binding. The inhibitory α-helix (α_{inh}) is either located on a separate protein that forms a tight toxin/antitoxin complex with the Fic enzyme (16) or at the N- or C-terminal position within the same polypeptide chain. These three possibilities lead to a classification of Fic proteins into classes I, II, and III, respectively (8). Mutation of the inhibitory Glu to Gly relieves autoinhibition, thus boosting both target and autoadenylylation (8, 9). However, the identity of the intrinsic or extrinsic factors that in vivo expulse the inhibitory Glu of α_{inh}, and thereby relieve autoinhibition, has not been investigated.

Fic proteins have evolved in bacteria and have spread by horizontal gene transfer into all domains of life (17). Despite structural conservation of the basic FIC-domain fold, there is significant sequence diversity among class I and II Fic proteins. Additionally, these two classes are frequently combined with other protein domains toward multidomain arrangements, demonstrating a high functional plasticity and adaptability (2). In contrast, class III Fic proteins are highly conserved single-domain proteins even though they are found scattered across all classes of Proteobacteria (8). This conservation suggests that class III Fic proteins are stand-alone autoregulated functional entities that act in a plug-and-play manner upon acquisition by horizontal gene transfer.

Here, we dissect the regulatory mechanism of NmFic from *Neisseria meningitidis* as representative for the class III Fic proteins. First, we identify the B-subunit of DNA gyrase as the main

Significance

FIC-domain enzymes are found in all kingdoms of life and catalyze posttranslational modifications of various target proteins to modulate their function. Because the vast majority of Fic proteins are expressed in an inhibited form, their physiological importance has escaped attention for a long time. This article reveals an autonomous mechanism of inhibition relief for class III Fic proteins, which hinges on autoadenylylation of an inhibitory helix. Because the process occurs *in cis*, the Fic enzyme constitutes a molecular timer that operates independent of enzyme concentration. Furthermore, we show that Fic-mediated adenylylation of DNA gyrase leads to bacterial growth arrest. Thus, the time-dependent inactivation of DNA gyrase may serve as a switch to bacterial dormancy under starvation or other stress conditions.

Author contributions: F.V.S., B.M.B., A.H., H.A., A.M., T. Sharpe, C.D., S.H., and T. Schirmer designed research; F.V.S., B.M.B., A.H., H.A., A.M., and T. Sharpe performed research; F.V.S., B.M.B., A.H., T. Sharpe, C.D., S.H., and T. Schirmer analyzed data; and F.V.S., B.M.B., A.H., T. Sharpe, C.D., S.H., and T. Schirmer wrote the paper.

The authors declare no conflict of interest.

This article is a PNAS Direct Submission. A.M. is a guest editor invited by the Editorial Board.

Freely available online through the PNAS open access option.

Data deposition: Coordinates and structure factors have been deposited in the Protein Data Bank, www.pdb.org (PDB ID codes 5CGL, 5CKL, and 5CMT). Sequence-specific resonance assignments have been submitted to the Biological Magnetic Resonance Data Bank (accession code 26607).

[1]To whom correspondence may be addressed. Email: christoph.dehio@unibas.ch, sebastian.hiller@unibas.ch, or tilman.schirmer@unibas.ch.

This article contains supporting information online at www.pnas.org/lookup/suppl/doi:10.1073/pnas.1516930113/-/DCSupplemental.

bacterial target of NmFic, as for class I Fic proteins (5). We then reveal the crucial role of autoadenylylation in the activation of class III Fic proteins and the opposing role of oligomerization, resulting in a peculiar and intriguing NmFic concentration dependence of target adenylylation. Ultimately, because the oligomerization interfaces are either highly conserved or covaried, and because the modifiable residue Y183 is strictly conserved in class III Fic proteins, we anticipate that the combination of oligomer dissociation and subsequent *cis*-autoadenylylation is the major regulatory mechanism of class III Fic proteins.

Results

NmFic Adenylylates DNA Gyrase. We have previously shown that expression of inhibition-relieved mutants of various bacterial Fic proteins slowed down the growth of ectopically expressing *Escherichia coli* (8). This growth reduction correlated with in vitro adenylylation of an endogenous protein with a mass of about 90 kDa. Subsequently, it was shown that the class I Fic protein VbhT adenylylates the B-subunit of the bacterial topoisomerases DNA gyrase (GyrB) and topoisomerase IV (ParE) (5). The modification affects a conserved Tyr of the ATP binding-site lid, thus interfering with ATPase and topoisomerase activity.

Because expression of (class III) NmFic in its inhibition-relieved form ($NmFic_{E186G}$) also slows down *E. coli* growth (8), we tested whether NmFic modifies the same targets (Fig. 1). Corroborating our previous findings (8), $NmFic_{wt}$ does not adenylylate any of the target proteins. In contrast, $NmFic_{E186G}$ efficiently adenylylates *N. meningitidis* GyrB and the orthologous *E. coli* and *Mycobacterium tuberculosis* proteins, but not ParE of *N. meningitidis* or *E. coli*. Mutation of the *E. coli* GyrB acceptor site (Y109F or Y109A variant) completely abrogates the effect (Fig. 1), confirming the predicted modification. In addition, independent of the presence of the target, strong autoadenylylation of $NmFic_{wt}$ and $NmFic_{E186G}$ is observed (Fig. 1), which is investigated further below.

Conserved Tetrameric Organization of Class III Fic Proteins. NmFic invariably shows a tetrameric arrangement (Fig. 2 and Fig. S1) in different crystal forms and ligation states, even when the C-terminal helix is absent or disordered (Fig. S1 *A–C*). The tetramer is of 222 symmetry (dimer of dimers), and its formation involves two independent interfaces (Fig. 2 *A–C* and Movie S1). Interface 1 is mainly mediated by the apolar interactions of F70 and Y77, with their respective symmetry mates, and by R71 and E102, which form two isologous salt bridges (Fig. 2*B*). The interface 1 residues are strongly conserved among the 197 analyzed sequences of class III Fic proteins. Similarly, interface 2 is formed by apolar residues L155 and F159, as well as the two isologous salt bridges of R149 and E156 (Fig. 2*C*). These residues are not strongly conserved, but the interacting residues show strong covariation with the striking charge reversal of the E-R to K-E salt bridges in a subset of the class III proteins. Taken together, conservation and covariance of the surface residues of NmFic suggest that tetramer formation is of functional importance for class III Fic proteins.

To describe the stability of the tetramer in solution, we determined the dissociation constants by performing size exclusion chromatography coupled to multiangle laser light scattering (SEC-MALLS; Fig. 2*D*, *Top*) and analytical ultracentrifugation sedimentation velocity (AUC-SV), using partially fluorescein-labeled protein (Fig. 2*D*, *Bottom*) measurements at varying protein concentrations. The observed shift of apparent molecular mass and elution volume with protein concentration in SEC-MALLS (Fig. S2*A*) indicated an oligomer equilibrium with fast kinetics relative to the duration of an SEC run. Nonlinear least squares fit of the data with an appropriate thermodynamic model (Fig. S3 *A* and *B*) yielded the dissociation constants $K_{d,1}$ and $K_{d,2}$ for the two independent interfaces. For $NmFic_{wt}$, both values are in the low micromolar range (Table 1). Interestingly, addition of the ATP substrate stabilized the tetramer considerably (Fig. 2*D*, *Bottom*, and Table 1).

To test whether the crystallographically observed tetramer also occurs in solution and whether it is of physiological relevance, we generated NmFic variants with single point mutations in one or both of the interfaces. Based on the crystal structure, charge reversal mutations E102R and E156R were expected to disrupt interfaces 1 and 2, respectively. Indeed, $NmFic_{E102R}$ and $NmFic_{E156R}$ do not form tetramers but exhibit a concentration-dependent monomer/dimer equilibrium (Fig. 2*D*). Furthermore, the dimer dissociation constants of the two variants agree very well with the dimer dissociation constants obtained from the fit of the $NmFic_{wt}$ tetramerization data (Table 1), indicating that the two interfaces are not allosterically coupled. In addition, the crystal structures of $NmFic_{E102R}$ and $NmFic_{E156R}$ (Fig. S2 *B–E* and Table S1) revealed virtually identical interfaces to the interfaces present in the tetrameric WT protein (Fig. S2 *B–E*). Finally, combination of both mutations in $NmFic_{E102R,E156R}$ yielded an oligomerization-deficient monomeric mutant $NmFic_{mono}$, with a concentration-independent mass identical to the theoretical mass of the monomer (Fig. 2*D*).

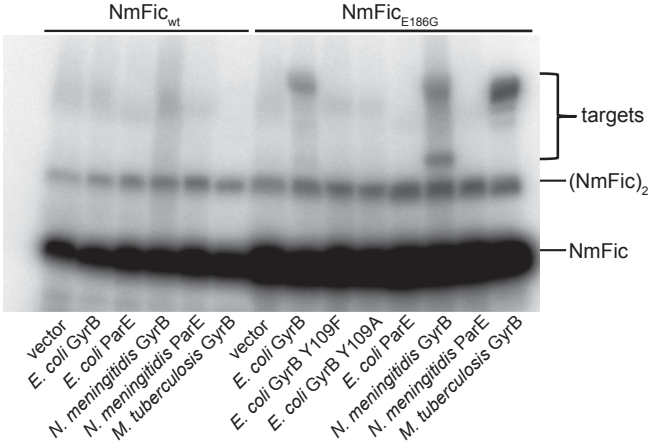

Fig. 1. $NmFic_{E186G}$ adenylylates GyrB. Autoradiographs obtained after incubation of $NmFic_{wt}$ (*Left*) and inhibition-relieved variant $NmFic_{E186G}$ (9) (*Right*) with 40 nM α-[^{32}P]ATP, 15 mM $MgCl_2$, and *E. coli* cell lysates overexpressing potential targets as indicated. Incubation was for 1 h at 30 °C.

Disruption of the Tetramer Activates NmFic. To obtain insight into the physiological role of oligomerization, the tetramerization-deficient mutants were assayed in vivo. Taking a derivative of *E. coli* K12 MG1655 (AB472) as a model organism (8), the bacterial growth inhibition upon expression of NmFic variants was assessed on LB-agar plates supplemented with increasing amounts of isopropyl β-D-thiogalactopyranoside (IPTG; up to 2 mM) as a physiological readout for gyrase inactivation. Fig. 3*A* shows the quantification of bacterial growth by counting colony-forming units (CFU; also Fig. S4 *A* and *B*).

In contrast to WT NmFic, the tetramerization-deficient mutants $NmFic_{E102R}$, $NmFic_{E156R}$, and $NmFic_{E102R,E156R}$ showed a severe, IPTG-dependent, growth defect (Fig. 3*A*), resulting in the loss of almost 1.5, 3.0, and 1.5 $\log_{10}$ CFU/mL viability, respectively. In addition to the strongly reduced numbers, the colonies exhibited a drastically smaller size (Fig. S4*B*). As expected, by additional mutation of the catalytic His (H107A), the observed growth defect was completely abolished (Fig. 3*A*), demonstrating that the phenotype depends on the catalytic activity of NmFic. As expected, the observed *E. coli* growth defect correlates very well with GyrB43 adenylylation, as assayed in vitro by autoradiography (Fig. 3*B*). Again, the combination of the interface mutations

with H107A completely suppressed both autoadenylylation and target adenylylation.

Although all tested interface mutants are active, $NmFic_{E102R}$ and $NmFic_{E102R,E156R}$ show lower activity than $NmFic_{E156R}$. An explanation for this reduced activity may be that the strictly conserved acidic residue 102, which is replaced in both mutants, may contribute to the recognition of the target protein GyrB. Note that the autoadenylylation efficiency is very similar for all oligomerization-deficient mutants (Fig. 3 *B* and *E*), suggesting that the active center, per se, is unperturbed. In summary, the results indicate that NmFic tetramerization renders the enzyme incompetent for efficient autoadenylylation and for target adenylylation.

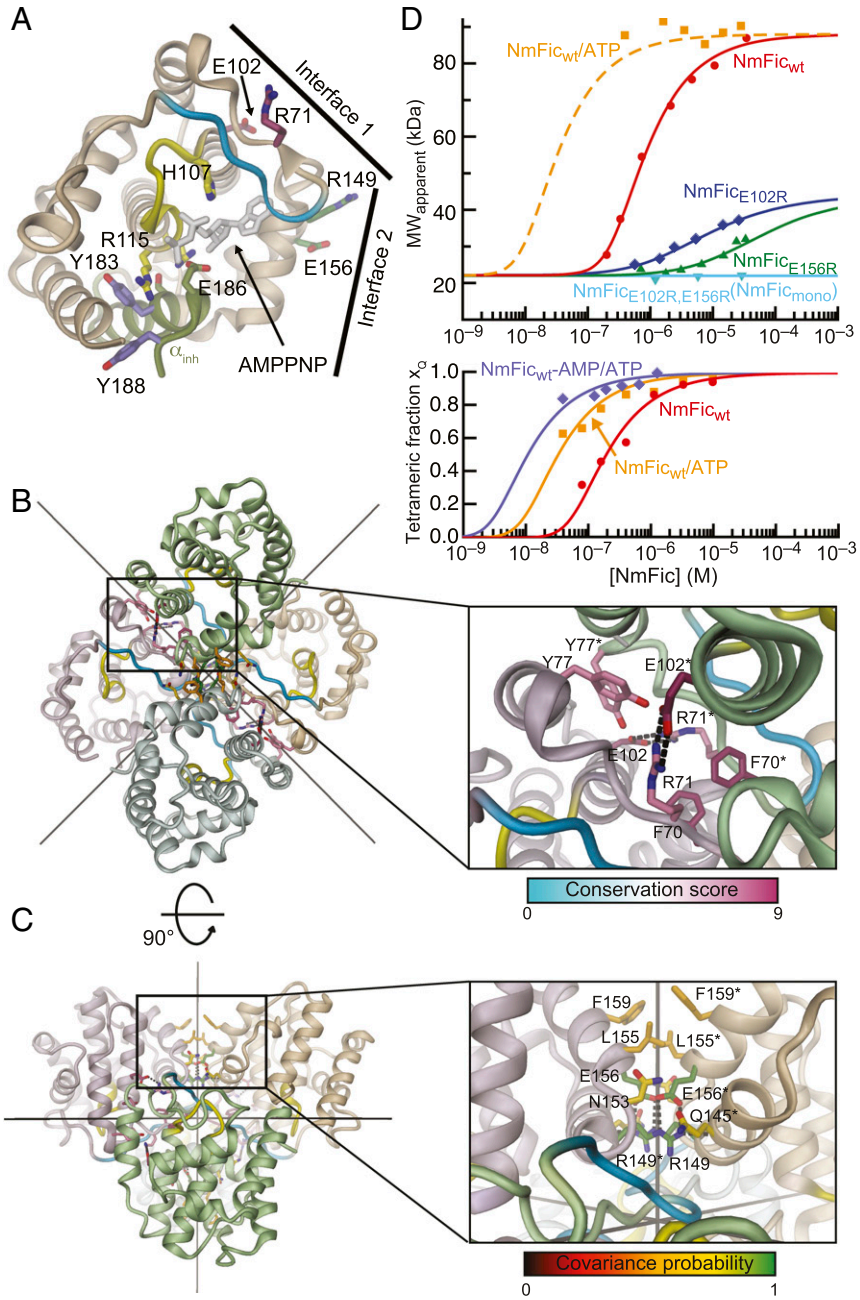

Fig. 2. Structural and oligomeric analysis of NmFic. (*A*) Cartoon of the NmFic structure (PDB ID code 3S6A) with the active site motif highlighted in yellow and the target binding site (flap) in blue. Important residues are shown in full with side-chain carbon atoms of active site residues colored in yellow, modifiable Tyr in purple, and charged residues mediating oligomerization in magenta (interface 1) and green (interface 2). The α_{inh} is shown in olive-green with the inhibitory Glu (E186) shown in full. (*B*) View of the crystal structure of the NmFic tetramer (222 symmetry with the twofold axes indicated) with the subunits distinguished by color (*Left*) and close-up views of the dimerization interface 1, with a contact area of 835 $Å^2$ (*Right*). Side-chain carbon atoms are colored according to the conservation score [ConSurf (28)]. (*C*) Ninety-degree rotation of the crystal structure shown in *B* (*Left*) and close-up view of the dimerization interface 2, with a contact area of 425 $Å^2$ (*Right*). Side-chain carbon atoms are colored according to covariance probability [Gremlin (29)]. In *B* and *C*, asterisks denote residues from the neighboring molecule. (*D*) Dynamic oligomerization equilibrium of $NmFic_{wt}$ and variants. (*Top*) Concentration dependence of the apparent molecular weight as determined by SEC-MALLS for $NmFic_{wt}$ and oligomerization interface variants. (*Bottom*) Tetrameric fraction x_Q of $NmFic_{wt}$ in the absence and presence of 5 mM ATP and autoadenylylated $NmFic_{wt}$-AMP in the presence of 5 mM ATP. The lines represent the nonlinear least squares fitting of the monomer/oligomer equilibria according to the model shown in Fig. S3*A*. Resulting dissociation constants are shown in Table 1.

Table 1. Biophysical characterization of NmFic oligomerization

NmFic variants and conditions	Method	$K_{d,1}$, μM	$K_{d,2}$, μM	$K_{d,2'}$, μM
$NmFic_{E102R}$	MALLS	7.4 ± 1.1	—	—
$NmFic_{E156R}$	MALLS	—	60 ± 12	—
$NmFic_{wt}$	MALLS	7.6 ± 1.1	61 ± 9	—
$NmFic_{wt}$*	AUC	2.6 ± 0.1	20	—
$NmFic_{wt}$ (5 mM ATP)*	AUC	0.71 ± 0.04	5.5	—
$NmFic_{wt}$-AMP (5 mM ATP)†	AUC	0.71	—	1.1 ± 0.2

Oligomerization parameters were fitted according to the kinetic scheme (Fig. S3*A*) to the data shown in Fig. 2*D*. $K_{d,1}$ and $K_{d,2}$ correspond to the dissociation constants for NmFic dimerization via interfaces 1 and 2, respectively.

*Due to the limited amount of data points, only one of the dissociation constants ($K_{d,1}$) was fitted and the other ($K_{d,2}$) was computed, keeping $K_{d,2}/K_{d,1} = 7.7$, based on the ratio obtained for $NmFic_{wt}$.

†Based on structural considerations, it can be assumed that the autoadenylylated C-terminal segment does not affect interface 1. Therefore, $K_{d,1}$ was set to the value obtained for the nonmodified protein, and only $K_{d,2'}$ was fitted (Fig. S3*C*).

NmFic Autoadenylylates a Buried Tyr *in Cis*. Automodification has been observed for most Fic proteins described to date (6, 8–15). For NmFic, the sites of autoadenylylation have been mapped to Y183 and Y188 of the α_{inh} by mass spectrometry (MS) (8) (Fig. 2*A*, purple residues). Intriguingly, and in contrast to Y188, the strictly conserved Y183 is completely buried in the hydrophobic core of the protein. Therefore, it can be inferred that the α_{inh} has to detach from the core of the protein for the Y183 adenylylation reaction to occur. Furthermore, for steric reasons, the α_{inh} would no longer be able to repack after modification.

Autoadenylylation of NmFic was monitored in real-time by circular dichroism (CD) spectroscopy. Because $NmFic_{wt}$ shows little autoadenylylation (Fig. 3*B*), we used $NmFic_{mono}$ ($NmFic_{E102R,E156R}$) for this and the following analyses. Upon addition of ATP/$MgCl_2$, the CD spectrum of $NmFic_{mono}$ showed a gradual, time-dependent decrease in amplitude of the negative peaks at 208 and 222 nm (Fig. S5*A*), corresponding to a reduction of α-helical content. This decrease is entirely consistent with (partial) unfolding of the α_{inh} upon autoadenylylation.

As another readout of autoadenylylation, the thermal stability of $NmFic_{mono}$, was monitored by differential scanning fluorimetry (DSF; Fig. S5*B*). The modification resulted in significant destabilization of the protein (decrease in melting temperature of 8 °C), consistent with the partial loss of secondary structure shown above and the concomitant loss of packing interactions. Importantly, the reaction kinetics were found to be independent of the NmFic concentration, indicating that the reaction takes place *in cis*. The data obtained at various $NmFic_{mono}$ concentrations (Fig. 4) could indeed be fitted globally with one apparent first-order rate constant, $k_{cat,1}$ (Table 2). Structural modeling verified that upon α_{inh} unfolding, the disordered C-terminal segment is long enough to allow Y183 to reach the target dock of the same molecule. A model of the structural changes accompanying NmFic autoadenylylation is shown in Movie S2.

Additionally, we tested whether the $NmFic_{mono,H107A}$ mutant, which is catalytically inactive and thus incompetent for *cis* modification, can be modified *in trans*. In mixtures of $NmFic_{mono}$ and $NmFic_{mono,H107A}$, the final concentration of the adenylylated product was found to correspond closely to the final concentration of the active $NmFic_{mono}$ enzyme only (Fig. S5*C*). This observation corroborates the conclusion that autoadenylylation occurs *in cis*.

Ultimately, we subjected our samples to MS analyses (Fig. S6 *A* and *B*). Indeed, $NmFic_{mono,H107A}$ showed the native mass, confirming that $NmFic_{mono}$ is not able to catalyze the modification of the inactive mutant *in trans*. In contrast, the mass of $NmFic_{mono}$ was increased by 1,316 Da, corresponding to the mass of four AMP moieties. Thus, apart from the already identified Tyr residues Y183 and Y188, the presence of two more acceptor sites can be inferred. The MS analysis was also performed on $NmFic_{mono,Y183F}$ (in the presence of $NmFic_{mono}$) and revealed two species corresponding to doubly and triply modified protein. As anticipated, we did not observe modification on four sites because the main acceptor site Y183 had been mutated in this protein variant. Furthermore, the Y183F mutation appears to slow down autoadenylylation (also Fig. 3*G*), because the automodification reaction did not reach completion (triply modified $NmFic_{mono,Y183F}$). Reduced autoadenylylation of the $NmFic_{mono,Y183F}$ mutant compared with $NmFic_{mono}$ was also observed by autoradiography (Fig. S6 *C* and *D*). Finally, residues Y184 and Y185 were identified as the remaining acceptor sites, because the mutant having all four Tyr residues (Y183, Y184, Y185, and Y188) replaced by Phe showed virtually no autoadenylylation. Satisfactorily, the sequential removal of individual acceptor sites in the combinatorial mutants resulted in a linear decrease of the band intensity on the autoradiographs (Fig. S6 *C* and *D*).

α_{inh} of Autoadenylylated NmFic Is Partly Unfolded. We further investigated the structural changes accompanying NmFic automodification by high-resolution nuclear magnetic resonance (NMR) spectroscopy (Fig. 5). We obtained well-dispersed NMR spectra for an unmodified protein (catalytically inactive $NmFic_{mono,H107A}$), as well as for autoadenylylated ($NmFic_{mono}$-AMP) protein. Sequence-specific backbone resonance assignments were obtained for 96% of the residues of $NmFic_{mono,H107A}$ (Fig. S7*A*). Based on these assignments, the chemical shifts of the autoadenylylated form could be assigned to 91% and confirmed by additional triple-resonance experiments. The overlay of the 2D [^{15}N,^{1}H]-HSQC (heteronuclear single quantum coherence) spectra of the native and autoadenylylated proteins shows large chemical shift differences for a subset of resonances (Fig. 5*A*). The residue-specific analysis of chemical shift changes upon autoadenylylation (Fig. 5 *B* and *C*) revealed that helix 8 (α_{inh}) is the most affected region of the protein. Therein, the covalently adenylylated residue Y183 showed the most pronounced chemical shift change [$\Delta\delta$(HN) = 6.7 ppm]. Furthermore, the amide chemical shifts of residues 178–191 populate the random coil region (7.5–8.5 ppm), indicating an unfolded conformation. In addition, the target-binding site (flap) and helix 1 (adjacent to helix 8) show significant chemical shift differences, but to a lesser extent than the α_{inh}, and a few residues in these regions are broadened beyond detection (Fig. 5*B*). Due to the point mutation H107A in the native form, the active site region also shows some chemical shift differences (Fig. 5 *B* and *C*). Despite these changes, the structural scaffold of the protein remains intact upon autoadenylylation. To characterize the secondary structure elements of both NmFic forms in solution, we used the secondary chemical shifts of the backbone ^{13}Cα nuclei (Fig. 5*D*). In aqueous solution, $NmFic_{mono}$ features eight α-helices, which agree in number and positioning with the crystal structure. The picture changes for the autoadenylylated form, in which the first seven helices are maintained, whereas the α_{inh} features helical structure only in its first two helical turns, but is unfolded from the position of residue G178 onward. These secondary structure changes are in full agreement with the chemical shift perturbation in 2D [^{15}N,^{1}H]-HSQC spectra (Fig. 5*D* and Movie S2). Overall, these data confirm the hypothesis that the α_{inh} cannot adopt its original position and conformation upon autoadenylylation of Y183.

NmFic Autoadenylylation Relieves Autoinhibition. We have shown that *cis*-autoadenylylation of NmFic constitutes an in-built mechanism to covalently modify Y183, resulting in partial unfolding of the α_{inh}. Obviously, this modification should be of functional relevance, considering that the α_{inh} in its native form partially

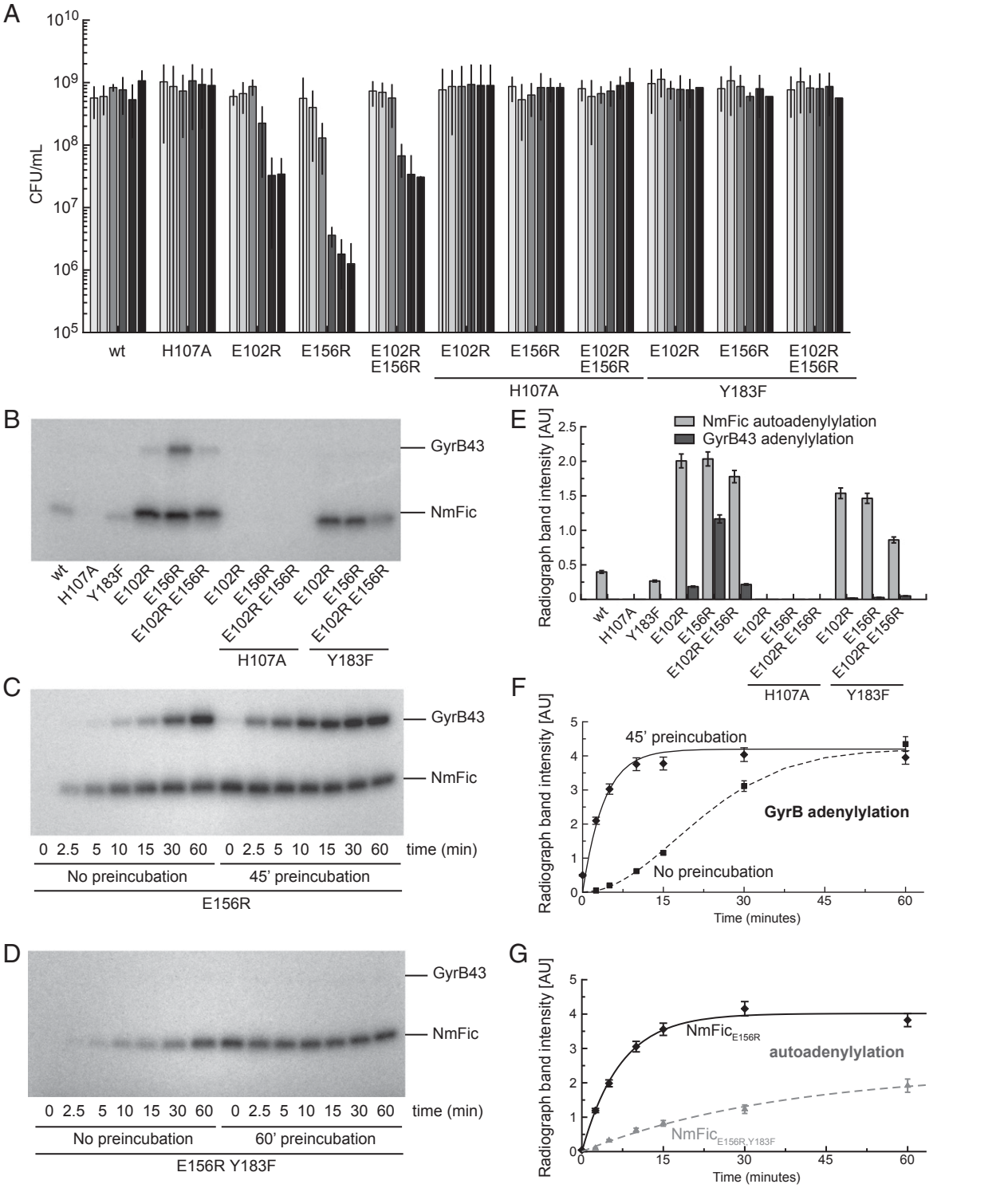

Fig. 3. Activation of NmFic leads to *E. coli* growth defect and in vitro adenylylation of GyrB. (*A*) Quantification of *E. coli* growth upon repression (1% glucose) or induction of the expression of NmFic variants at varying inducer (IPTG) concentrations from a single-copy plasmid (left to right with a color gradient from white to black: 1% glucose, no IPTG, 100 μM IPTG, 500 μM IPTG, 1 mM IPTG, 2 mM IPTG). The bars represent the average of three independent experiments, and error bars represent the SD. Note the remarkable growth defect of mutants NmFic$_{E102R}$, NmFic$_{E156R}$, and NmFic$_{E102R,E156R}$ (NmFic$_{mono}$). Raw data for 1% glucose and 2 mM IPTG are shown in Fig. S4 *A* and *B*. (*B–D*) Autoradiographs obtained after incubation of various NmFic mutants with 25 nM α-[^{32}P]ATP, 5 mM ATP, 10 mM $MgCl_2$, and purified GyrB43 (N-terminal GyrB 43-kDa fragment comprising the ATPase and transducer domains) at 35 °C. (*B*) In vitro adenylylation assay with 1 μM purified NmFic and 2.5 μM purified GyrB43 using an incubation time of 1 h. (*C*) Time course of autoadenylylation and GyrB43 adenylylation by NmFic$_{E156R}$ with or without ATP preincubation using 1 μM NmFic$_{E156R}$ and 5 μM GyrB43. Note that adenylylation of GyrB43 is delayed without preincubation (i.e., activation) of the Fic enzyme. (*D*) Same as in *C*, but for NmFic$_{E156R,Y183F}$. Note that this mutant is unable to adenylylate GyrB43. (*E–G*) Quantification of the radiograph band intensities shown in *B–D*. The assumed error of 5% is depicted as error bars. (*E*) Bar diagram representing NmFic autoadenylylation (light gray) and GyrB43 adenylylation (dark gray) catalyzed by the NmFic variants. (*F*) Time course of GyrB43 adenylylation with or without preincubation of NmFic$_{E156R}$. Also shown are the simulated curves obtained by global fitting of the kinetic model shown in Fig. 6*A* to the data. Resulting parameters are given in Table 2. (*G*) Time course of autoadenylylation of NmFic$_{E156R}$ and NmFic$_{E156R,Y183F}$. Fitting analogously to *F* yielded apparent $k_{cat,1}$ values of 2.4 * 10^{-3}·s^{-1} and 4.5 * 10^{-4}·s^{-1}, respectively. AU, arbitrary units.

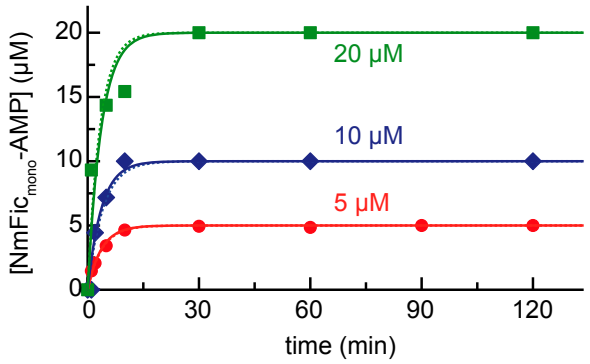

Fig. 4. *Cis*-autoadenylylation of monomeric NmFic. Progress curves of autoadenylylation of NmFic$_{mono}$ acquired at the indicated protein concentrations using 5 mM ATP and 10 mM $MgCl_2$. The data were fitted to a first-order reaction model. Dotted lines are the result of individual fitting, and plain lines are the result of global fitting of the three independent experiments (apparent $k_{cat,1}$ of 4.5 * 10^{-3}·s^{-1}; Table 1). Note that individual and global fitting are virtually identical.

obstructs the nucleotide binding site, and thereby autoinhibits Fic enzymes (8). Thus, to test for any functional role of Y183, we removed its hydroxyl group by introducing an additional Y183F mutation into the alleles of active (i.e., oligomerization-deficient), mutants. Strikingly, the mutation suppressed the growth defect phenotype as efficiently as mutation of the catalytic His (H107A) (Fig. 3*A*, *Right*), suggesting a crucial regulatory role for Y183.

The in vivo observation was faithfully mirrored in the autoradiograph obtained after incubation of the various purified NmFic mutants with radioactive ATP (Fig. 3*B*). In vitro GyrB43 adenylylation, which is efficiently catalyzed by the three interface mutants (Fig. 3*B*, lanes 4–6), is almost completely abolished in their respective Y183F variants (Fig. 3*B*, lanes 10–12).

The remaining autoadenylylation of the Y183F NmFic variants (Fig. 3*B*, *Right*), which is due to the modification of Y184, Y185, and Y188, indicates that enzyme function, per se, is not impaired. As expected, no target adenylylation is observed. Thus, (partial) modification of the additional Tyr residues does not significantly relieve autoinhibition. Still, to corroborate that the Y183F mutation had no unforeseen effect on the enzyme, we determined the high-resolution (0.99 Å) crystal structures of both NmFic$_{E156R}$ and NmFic$_{E156R,Y183F}$ (Fig. S4 *C* and *D*). Indeed, the structures are virtually identical, apart from the absence of the Y183 hydroxyl group in the double mutant.

To test whether the kinetics of autoadenylylation and target adenylylation would be of physiological relevance, we measured time courses of product (GyrB-AMP) formation for NmFic$_{E156R}$ (Fig. 3*C*). The apparent rate of NmFic$_{E156R}$ autoadenylylation derived from Fig. 3*G* agrees well with the one obtained for NmFic$_{mono}$ by DSF analysis (Table 2). Similarly, NmFic$_{E156R,Y183F}$ shows autoadenylylation, although with a considerably slower rate (Fig. 3 *D* and *G*). Such an effect of the Y183F mutation was also observed for NmFic$_{mono,Y183F}$ by MS (Fig. S6*B*). As mentioned above, the modification on residues Y184, Y185, and Y188 is probably not of functional relevance.

Under the used conditions, NmFic$_{E156R}$ fully converts GyrB43 to its adenylylated form within 1 h (Fig. 3 *C* and *F*), but with a pronounced lag phase. This delay is absent in the progress curve of preactivated Fic enzyme, which suggests again that only the adenylylated form is catalytically active. This interpretation was confirmed quantitatively by globally fitting the respective kinetic model (Fig. 6*A*, but without oligomerization) to the data (Fig. 3*F*). Upon setting $K_{m,GyrB}$ to the experimentally determined value of 39 μM, the fit yielded the turnover numbers of autoadenylylation ($k_{cat,1,eff}$) and target adenylylation ($k_{cat,2}$) given in Table 2. Notably, $k_{cat,1,eff}$ turned out to be about one order of magnitude slower that the corresponding rate, $k_{cat,1}$, as measured by DSF. Therefore, it can be concluded that the rate-determining step of Fic activation is the debinding of the modified segment from the active site ($A^0 \rightarrow A$).

Activity Profile of NmFic$_{wt}$ Is a Consequence of Autoactivation Combined with Oligomerization. We have thus shown that NmFic-catalyzed target adenylylation is controlled by enzyme tetramerization as well as *cis*-autoadenylylation. These results were obtained by analyses of mutants deficient in one or the other function. What, then, would be the combined effect in the WT enzyme? Fig. 6*B* shows the autoradiographs obtained after incubation of NmFic$_{wt}$ (at varying concentrations) with GyrB43 for various durations. At the standard enzyme concentration of 1 μM, weak NmFic$_{wt}$ autoadenylylation and no significant target adenylylation are observed for incubation times up to 8 h, consistent with our earlier result (Fig. 3*B*, first lane). Strikingly, strong GyrB43 adenylylation is observed at lower enzyme concentrations (250 nM and lower), with an abrupt transition from 250 to 500 nM. Because this transition occurs in a very similar range as the monomer-to-tetramer transition (Fig. 2*D*, *Bottom*), it most probably reflects the emergence of catalytically incompetent tetramers at higher concentrations.

Importantly, however, the catalytic incompetence of the tetramer alone is not sufficient to explain the data, because not only the tetramer/monomer ratio but also the absolute concentration of active monomers will increase with total concentration (Fig. S2*H*). To rationalize the observed effects quantitatively, we set up a kinetic scheme including autoactivation and inactivation by oligomerization as shown in Fig. 6*A* (also Fig. S3*C*). In this model, autoinhibited native NmFic (N) is in equilibrium with states N′ (α_{inh} unfolded) and N′′ (modifiable Y183 positioned in the active site). The latter state gets autoadenylylated at Y183 in a first-order reaction to yield A^0. Finally, unbinding of the modified C terminus will result in a monomer state A that is predicted to be

Table 2. Enzymatic characterization of NmFic-catalyzed autoadenylylation and target adenylylation

Reaction	Parameter	k_{cat}, s^{-1}	K_m, μM	Method
Autoadenylylation				
(N,N′,N′′) → (A^0,A)	$k_{cat,1}$	(4.5 ± 0.53) 10^{-3}	n/a	DSF (Fig. 4)
(N,N′,N′′) → (A^0,A)	$k_{cat,1}$	(2.3 ± 0.08) 10^{-3}	n/a	Adenylylation assay (Fig. 3*G*)
(N,N′,N′′) → A	$k_{cat,1,eff}$	(2.1 ± 0.25) 10^{-4}	n/a	Adenylylation assay (Fig. 3*F*)
Target adenylylation				
A + G → A + G-AMP	$k_{cat,2}$	0.18 ± 0.01		Adenylylation assay (Fig. 3*F*)
A + G → A + G-AMP	$K_{m,G}$		39.7 ± 3.6	Adenylylation assay (not shown)

All parameters are apparent parameters referring to an ATP concentration of 5 mM. The K_d of ATP binding to native monomeric NmFic has been measured by NMR to 7.8 mM (Fig. S7*C*). The value of $k_{cat,1}$ was determined by DSF and adenylylation assay for NmFic$_{mono}$ and NmFic$_{E156R}$, respectively. The values agree satisfactorily within a factor of 2. n/a, not applicable.

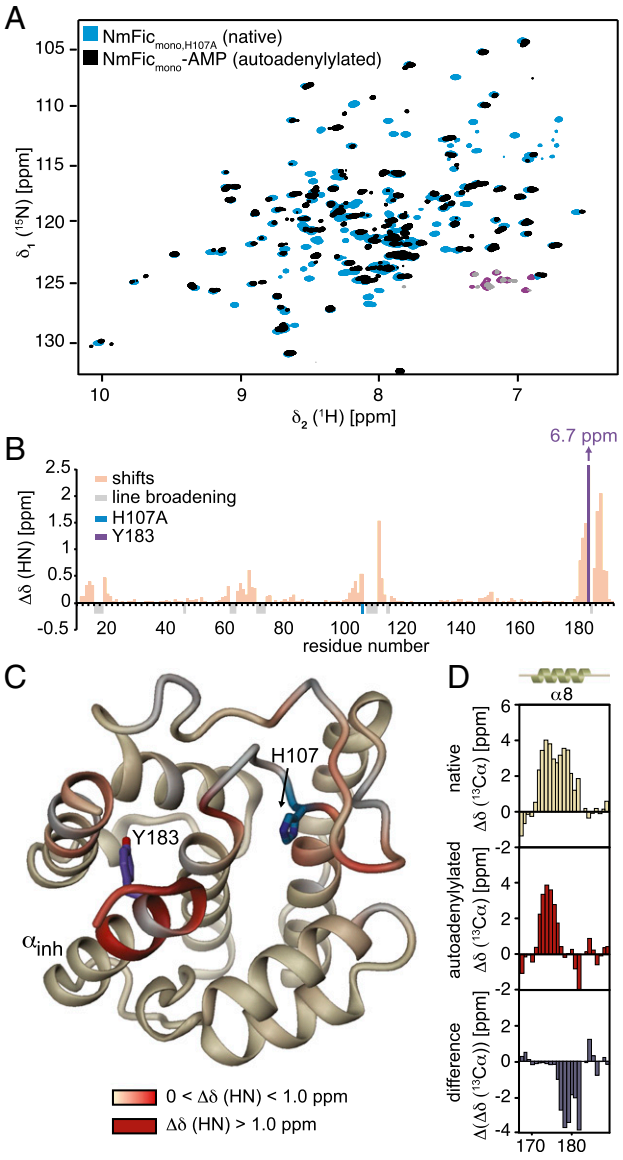

Fig. 5. Structural perturbations of NmFic upon autoadenylylation. (*A*) Overlay of 2D [^{15}N,^{1}H]-HSQC spectra of 500 μM [*U*-^{13}C,^{15}N]-labeled native inactive monomeric NmFic (NmFic$_{mono,H107A}$, cyan) and of 140 μM [*U*-^{13}C,^{15}N]-labeled autoadenylylated monomeric NmFic (NmFic$_{mono}$-AMP, black). (*B*) Amide-group chemical shift difference, Δδ(HN), between NmFic$_{mono,H107A}$ and NmFic$_{mono}$-AMP plotted as a function of NmFic residue number. Residues exhibiting significant line broadening in the adenylylated form are indicated in gray as negative bars. Values at positions 107 (H/A) and 183 (Y) are highlighted in blue and purple, respectively. (*C*) Amide-group chemical shift differences mapped on the structure of NmFic (PDB ID code 3S6A) using the indicated color code. The largest chemical shift differences cluster in helices α1 and α8 (α_{inh}) and in the flap region. (*D*) Secondary ^{13}Cα chemical shifts for residues 167–190 of native NmFic$_{mono,H107A}$ (*Top*), autoadenylylated NmFic$_{mono}$-AMP (*Middle*), and their difference (*Bottom*) relative to the random coil values. A 1-2-1 smoothing function was applied to the raw data. Consecutive stretches with positive and negative values indicate α-helical and β-strand secondary structure, respectively. The extent of α_{inh} as inferred from the crystal structure of the native NmFic is indicated on top. The full residue range is shown in Fig. S7*B*.

competent for target adenylylation. Note, that ATP binding will shift the $A^0 \Leftrightarrow A$ equilibrium toward the competent A state. Because monomers are in fast oligomerization equilibrium, active A monomers will repartition into the tetramer that acts as a reservoir, and will therefore be partly sequestered to the inactive oligomeric state.

We reasoned that a contribution of the unfolded autoadenylylated C-terminal segment to the interface might affect the oligomerization affinity. Indeed, in presence of 5 mM ATP, the dissociation constant ($K_{d,2'}$) of A was measured by AUC-SV to be fivefold lower than the corresponding constant of N (Fig. 2*D* and Table 1).

Using the experimentally determined parameters of the kinetic model (Tables 1 and 2), we then simulated GyrB43-AMP production as function of enzyme concentration and incubation time by numeric integration of the respective differential equations (Fig. 6 *C* and *D*). Indeed, as observed experimentally, target adenylylation efficiency drops with enzyme concentration above a certain threshold (Fig. 6*C*). Furthermore, the simulated progress curves (Fig. 6*D*) reproduce the lag phase observed at a high enzyme concentration. Taken together, the salient features of intrinsic NmFic regulation are faithfully captured by the proposed kinetic model.

Discussion

The physiological importance of AMP-transferases with FIC fold has escaped attention for a long time, because their activity is kept in check by intra- or intermolecular active site obstruction (8). In this study, we focused on class III Fic proteins that carry the inhibitory α_{inh} at the C terminus and are composed of a FIC domain only. We reveal that in addition to the previously reported autoinhibition (8), two further mechanisms inversely regulate adenylylation activity, namely, tetramerization and *cis*-autoadenylylation. This combination results in a complex autoregulatory mechanism.

NmFic forms a tetramer with the involved interfaces largely conserved or coevolved among class III members, suggesting conservation of the tetrameric arrangement in this class. Disruption of either interface was achieved by site-directed mutagenesis, thus verifying their role both in the crystalline state and the solubilized state. Due to the cooperative nature of tetramerization, a sharp monomer–tetramer transition occurs in the presence of ATP, at the rather low NmFic concentration of 50 nM (Fig. 2*D* and Fig. S2*G*). Clearly, the tetramer state is of physiological relevance, because expression of interface disruption mutants, but not of NmFic$_{wt}$, resulted in impaired growth of the expressing *E. coli* strain. Thus, it can be inferred that only monomeric NmFic is able to exert the growth retardation effect, which can be attributed to GyrB adenylylation (5). Most probably, the tetramer is catalytically noncompetent, because the binding site for the segment flanking the modifiable side chain [target dock (10)] is partially occluded. Furthermore, the strict conservation of oligomerization interface 1 (as opposed to interface 2, which shows covariation) may point to its involvement in mediating the contact between (monomeric) NmFic and the target. In fact, the surface-exposed area of the tetramer is highly variable, and therefore probably not involved in target recognition (Movie S1).

Fic automodification has been reported repeatedly (6, 8–15), but its role has remained unclear. In fact, nonspecific modification due to the high in vitro Fic concentrations used seemed possible. Here, we have shown that NmFic autoadenylylation crucially controls enzyme activity by relieving the autoinhibitory effect of the α_{inh}, as demonstrated by the Tyr-to-Phe mutation (Y183F) that fully suppressed the activating effect of the interface disruption mutants (Fig. 3*A*) and rendered the enzyme incompetent for target adenylylation (Fig. 3*B*). Biochemical and structural analyses confirmed that the conservative Y183F mutation does not disrupt the FIC fold (Fig. 3 and Fig. S4 *C* and *D*).

Importantly, the automodification occurs *in cis* with a reaction velocity independent of the total enzyme concentration. Indeed, structural modeling shows that upon unfolding of the α_{inh}, the modifiable Tyr can reach the active site of the same molecule (Movie S2). Probably, the segment flanking the Tyr residue would engage in β-strand interaction with the flap, resulting in

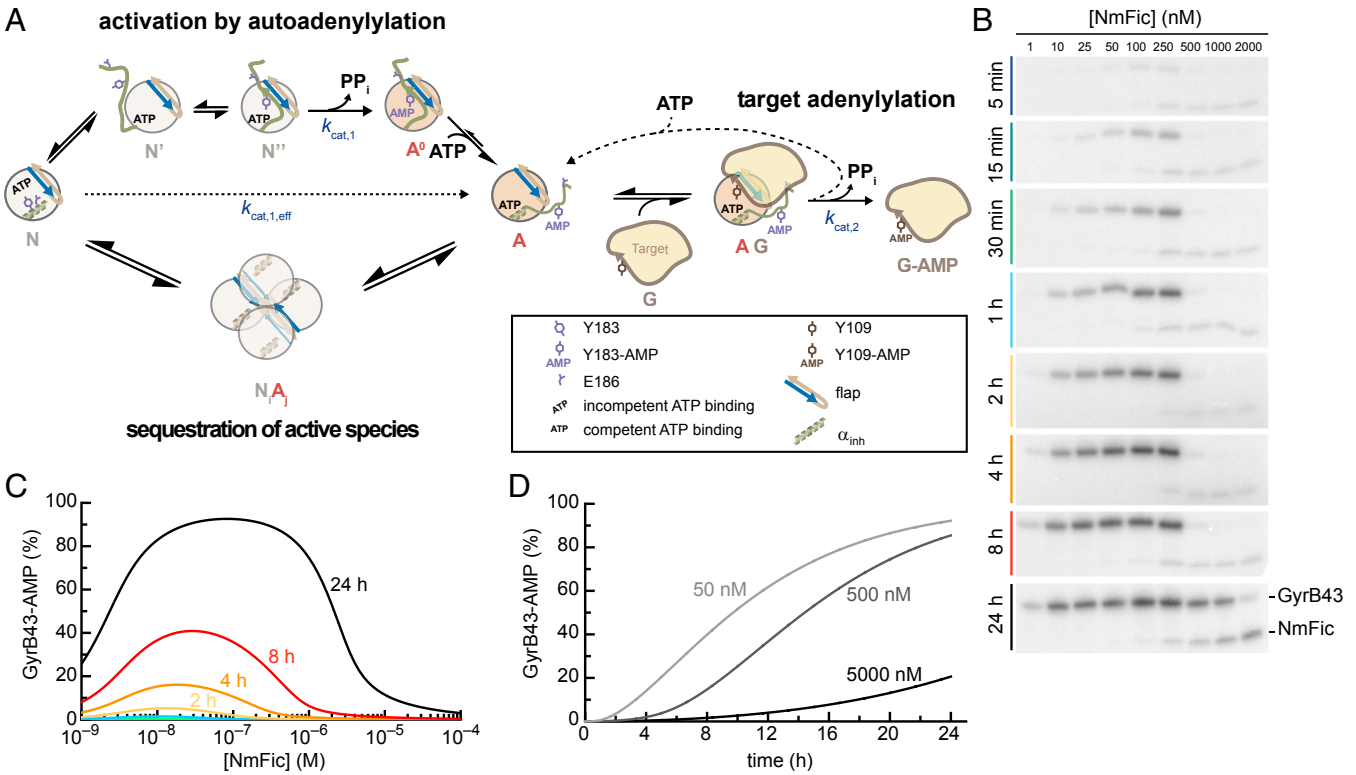

Fig. 6. Concentration and time dependence of NmFic$_{wt}$-catalyzed target adenylylation. (*A*) Simplified model of the regulatory mechanism of class III Fic proteins. (*Top Left*) Native monomeric Fic protein (N) is activated by autoadenylylation to yield A. This reaction involves unfolding of the α_{inh} (N′), binding of the modifiable Tyr Y183 of the unfolded segment to the flap (N′′), and subsequent autoadenylylation of Y183 (A^0). (*Bottom*) Both types of monomers (N and A) are in dynamic monomer/tetramer equilibrium to form homotetramers or heterotetramers N$_i$A$_j$, with i + j = 4. The tetramer acts as a buffer sequestering the active monomers. (*Right*) Only the remaining fraction of free (monomeric) A molecules is competent for target adenylylation. The complete model with all thermodynamic and kinetic parameters is shown in Fig. S3C. (*B*) Autoradiographs showing NmFic$_{wt}$ and GyrB43 adenylylation. The same experimental setup as in Fig. 3C was used but was carried out at various NmFic$_{wt}$ concentrations (1 nM to 2 μM, as indicated). Reactions were stopped after the indicated incubation times. (*C*) Simulation of GyrB adenylylation as a function of total NmFic$_{wt}$ concentration based on the kinetic model shown in *A* and Fig. S3C, with parameters set to their measured values (Tables 1 and 2). (*D*) Replot of the data shown in *C* as a function of incubation time for representative NmFic$_{wt}$ concentrations.

correct registration of the modifiable tyrosyl side-chain within the active site. This binding mode would be analogous to the one seen in the complex structures of IbpA$_{Fic2}$/cdc42 (6) and of noncognate peptide/Fic proteins (9). Because the flap is partially buried at the center of the tetramer, the structural model also explains why the tetramer would be incompetent for automodification. Thus, in the presence of ATP, native monomeric NmFic gets efficiently converted to its active, covalently modified form with a rather fast "in-built" first-order rate constant (Table 2, equivalent to a $t_{1/2}$ of about 150 s). As such, NmFic and, most likely, Fic proteins of class III in general constitute self-contained proteinaceous timers. Whether such an autoactivation mechanism also pertains to Fic proteins of class I and II remains to be seen, but conserved Tyr acceptor candidates can be identified in the N-terminal and central part of the fold, respectively. Noteworthy, *cis*-automodification has also been described for a few kinases as an activation mechanism (18).

The combination of the two coupled and counteracting effects, automodification and tetramerization, results in a quite unusual time and concentration dependence of target adenylylation, as captured in vitro by autoradiography (Fig. 6*B*) and reproduced *in silico* by respective simulations (Fig. 6 *C* and *D*). In essence (Fig. 6*A*), monomeric native Fic molecules (N) get converted with the intrinsic first-order rate to the autoadenylylated, active form (A). However, because Fic monomers are in fast equilibrium with the tetrameric state, they get redistributed such that the A/N ratio will be equal or larger in the tetrameric state. As a consequence, the increase in the absolute number of active monomers (A) will be dampened. Obviously, this buffering effect is most pronounced at high tetramer/monomer ratios (i.e., high enzyme concentrations) and will diminish when the autoadenylylation reaction reaches completion.

The comprehensive characterization of the complex autoregulatory mechanism of class III Fic proteins presented here sets the stage for future investigations of its physiological consequences. It has to be inferred, however, that the intrinsic regulatory mechanism may be further modulated by external factors, such as antagonistic phosphodiesterases [e.g., the de-AMPylase SidD of *Legionella* (19, 20)], specific proteases, or small ligands. Furthermore, Fic biosynthesis and degradation, as well as dilution effects during cell growth and division, will profoundly affect the time profile of the Fic pool activity. Still, solely based on the inherent mechanism, interesting consequences can be envisaged.

The nonmonotonic dependence of AMP-transferase activity on enzyme concentration would render the enzyme exquisitely sensitive to variation of its concentration in the bacterial cell. A twofold drop of NmFic concentration in the right range (e.g., due to cellular growth and division) would drastically increase catalytic activity, and thus GyrB inactivation. In addition, the considerable delay in NmFic-mediated GyrB adenylylation may be important in vivo to ensure that the growth-retarding effect of the target modification kicks in only under certain conditions, such as starvation, when synthesis of fresh NmFic has come to a halt. Molecular timers have been found before, such as the master regulator Spo0A of *Bacillus* that controls, upon phosphorylation, the switch from competence to sporulation via a well-characterized genetic circuit (21, 22) induced by prolonged times of nutriment

starvation. Class III Fic proteins may constitute a new family of molecular timers that are, in contrast to the master regulator Spo0A of *Bacillus*, fully autonomous and not relying on any feedback exerted by other components or a genetic circuit. This hypothesis will have to be tested in future studies.

Materials and Methods

Detailed information on cloning, expression, purification, crystallization, data collection, and structure determination by X-ray crystallography or NMR is provided in *SI Materials and Methods*. Plasmids were constructed as described previously (8, 23, 24) (Tables S2 and S3). Proteins were expressed and purified as described (8, 25). Toxicity tests and adenylylation assays were performed according to the protocols given by Harms et al. (5) and Goepfert et al. (9).

The oligomeric state of NmFic was determined by SEC-MALLS and AUC-SV at varying concentrations. DSF (26) was used to monitor in vitro autoadenylylation of NmFic. For simulations and fitting of functional data to the kinetic model, the programs ProFit 6.2.14 (QuantumSoft) and Complex Pathway Simulator (COPASI) 4.14 (27) were used.

Detailed information on the various experimental procedures is provided in *SI Materials and Methods*.

ACKNOWLEDGMENTS. We acknowledge Gerd Pluschke (Swiss Tropical and Public Health Institute) for kindly providing the genomic DNA of *N. meningitidis* 2808. We thank Tillmann Heinisch for help with MS analysis. We thank the staff of beamlines X06DA and X06SA of the Swiss Light Source for excellent support. This work was supported by the European Research Council Advanced Investigator Grant (ERC-2013-AdG) FICModFun 340330 (to C.D.) and Swiss National Science Foundation Grants 3100-132979 (to C.D.) and 31003A-138414 (to T. Schirmer).

1. Roy CR, Mukherjee S (2009) Bacterial FIC Proteins AMP Up Infection. *Sci Signal* 2(62): pe14.
2. Garcia-Pino A, Zenkin N, Loris R (2014) The many faces of Fic: Structural and functional aspects of Fic enzymes. *Trends Biochem Sci* 39(3):121–129.
3. Yarbrough ML, et al. (2009) AMPylation of Rho GTPases by *Vibrio* VopS disrupts effector binding and downstream signaling. *Science* 323(5911):269–272.
4. Worby CA, et al. (2009) The fic domain: Regulation of cell signaling by adenylylation. *Mol Cell* 34(1):93–103.
5. Harms A, et al. (2015) Adenylylation of Gyrase and Topo IV by FicT Toxins Disrupts Bacterial DNA Topology. *Cell Reports* 12(9):1497–1507.
6. Xiao J, Worby CA, Mattoo S, Sankaran B, Dixon JE (2010) Structural basis of Fic-mediated adenylylation. *Nat Struct Mol Biol* 17(8):1004–1010.
7. Luong P, et al. (2010) Kinetic and structural insights into the mechanism of AMPylation by VopS Fic domain. *J Biol Chem* 285(26):20155–20163.
8. Engel P, et al. (2012) Adenylylation control by intra- or intermolecular active-site obstruction in Fic proteins. *Nature* 482(7383):107–110.
9. Goepfert A, Stanger FV, Dehio C, Schirmer T (2013) Conserved inhibitory mechanism and competent ATP binding mode for adenylyltransferases with Fic fold. *PLoS One* 8(5):e64901.
10. Palanivelu DV, et al. (2011) Fic domain-catalyzed adenylylation: insight provided by the structural analysis of the type IV secretion system effector BepA. *Protein Sci* 20(3): 492–499.
11. Kinch LN, Yarbrough ML, Orth K, Grishin NV (2009) Fido, a novel AMPylation domain common to fic, doc, and AvrB. *PLoS One* 4(6):e5818.
12. Pieles K, Glatter T, Harms A, Schmidt A, Dehio C (2014) An experimental strategy for the identification of AMPylation targets from complex protein samples. *Proteomics* 14(9):1048–1052.
13. Feng F, et al. (2012) A *Xanthomonas* uridine 5′-monophosphate transferase inhibits plant immune kinases. *Nature* 485(7396):114–118.
14. Goody PR, et al. (2012) Reversible phosphocholination of Rab proteins by *Legionella pneumophila* effector proteins. *EMBO J* 31(7):1774–1784.
15. Bunney TD, et al. (2014) Crystal structure of the human, FIC-domain containing protein HYPE and implications for its functions. *Structure* 22(12):1831–1843.
16. Goepfert A, Harms A, Schirmer T, Dehio C (2013) Type II toxin-antitoxin loci: The fic family. *Prokaryotic Toxin-Antitoxins* (Springer-Verlag, Berlin Heidelberg), pp 177–187.
17. Khater S, Mohanty D (2015) In silico identification of AMPylating enzymes and study of their divergent evolution. *Sci Rep* 5:10804.
18. Lochhead PA (2009) Protein kinase activation loop autophosphorylation *in cis*: Overcoming a Catch-22 situation. *Sci Signal* 2(54):pe4.
19. Tan Y, Luo Z-Q (2011) *Legionella pneumophila* SidD is a deAMPylase that modifies Rab1. *Nature* 475(7357):506–509.
20. Chen Y, et al. (2013) Structural basis for Rab1 de-AMPylation by the *Legionella pneumophila* effector SidD. *PLoS Pathog* 9(5):e1003382.
21. Levine JH, Elowitz MB (2014) Polyphasic feedback enables tunable cellular timers. *Curr Biol* 24(20):R994–R995.
22. Levine JH, Fontes ME, Dworkin J, Elowitz MB (2012) Pulsed feedback defers cellular differentiation. *PLoS Biol* 10(1):e1001252.
23. Gotfredsen M, Gerdes K (1998) The *Escherichia coli* relBE genes belong to a new toxin-antitoxin gene family. *Mol Microbiol* 29(4):1065–1076.
24. Zheng L, Baumann U, Reymond J-L (2004) An efficient one-step site-directed and site-saturation mutagenesis protocol. *Nucleic Acids Res* 32(14):e115.
25. Stanger FV, Dehio C, Schirmer T (2014) Structure of the N-terminal Gyrase B fragment in complex with ADP·Pi reveals rigid-body motion induced by ATP hydrolysis. *PLoS One* 9(9):e107289.
26. Niesen FH, Berglund H, Vedadi M (2007) The use of differential scanning fluorimetry to detect ligand interactions that promote protein stability. *Nat Protoc* 2(9):2212–2221.
27. Hoops S, et al. (2006) COPASI–A COmplex PAthway SImulator. *Bioinformatics* 22(24): 3067–3074.
28. Ashkenazy H, Erez E, Martz E, Pupko T, Ben-Tal N (2010) ConSurf 2010: calculating evolutionary conservation in sequence and structure of proteins and nucleic acids. *Nucleic Acids Res* 38(Web Server issue):W529–W533.
29. Ovchinnikov S, Kamisetty H, Baker D (2014) Robust and accurate prediction of residue-residue interactions across protein interfaces using evolutionary information. *eLife* 3:e02030.
30. Reckel S, et al. (2010) Strategies for the cell-free expression of membrane proteins. *Methods Mol Biol* 607(Chapter 16):187–212.
31. Spirin AS, Baranov VI, Ryabova LA, Ovodov SY, Alakhov YB (1988) A continuous cell-free translation system capable of producing polypeptides in high yield. *Science* 242(4882):1162–1164.
32. Kabsch W (2010) XDS. *Acta Crystallogr D Biol Crystallogr* 66(Pt 2):125–132.
33. Evans PR, Murshudov GN (2013) How good are my data and what is the resolution? *Acta Crystallogr D Biol Crystallogr* 69(Pt 7):1204–1214.
34. McCoy AJ, et al. (2007) Phaser crystallographic software. *J Appl Cryst* 40(Pt 4):658–674.
35. Emsley P, Lohkamp B, Scott WG, Cowtan K (2010) Features and development of Coot. *Acta Crystallogr D Biol Crystallogr* 66(Pt 4):486–501.
36. Murshudov GN, et al. (2011) REFMAC5 for the refinement of macromolecular crystal structures. *Acta Crystallogr D Biol Crystallogr* 67(Pt 4):355–367.
37. Adams PD, et al. (2010) PHENIX: A comprehensive Python-based system for macromolecular structure solution. *Acta Crystallogr D Biol Crystallogr* 66(Pt 2):213–221.
38. Chen VB, et al. (2010) MolProbity: All-atom structure validation for macromolecular crystallography. *Acta Crystallogr D Biol Crystallogr* 66(Pt 1):12–21.
39. Glaser F, et al. (2003) ConSurf: Identification of functional regions in proteins by surface-mapping of phylogenetic information. *Bioinformatics* 19(1):163–164.
40. Pervushin K, Riek R, Wider G, Wüthrich K (1997) Attenuated T_2 relaxation by mutual cancellation of dipole-dipole coupling and chemical shift anisotropy indicates an avenue to NMR structures of very large biological macromolecules in solution. *Proc Natl Acad Sci USA* 94(23):12366–12371.
41. Sattler M, Schleucher J, Griesinger C (1999) Heteronuclear multidimensional NMR experiments for the structure determination of proteins in solution employing pulsed field gradients. *Prog Nucl Magn Reson Spectrosc* 34(2):93–158.
42. Zhu G, Xia Y, Nicholson LK, Sze KH (2000) Protein dynamics measurements by TROSY-based NMR experiments. *J Magn Reson* 143(2):423–426.
43. Lee D, Hilty C, Wider G, Wüthrich K (2006) Effective rotational correlation times of proteins from NMR relaxation interference. *J Magn Reson* 178(1):72–76.
44. Güntert P, Dötsch V, Wider G, Wüthrich K (1992) Processing of multi-dimensional NMR data with the new software PROSA. *J Biomol NMR* 2(6):619–629.
45. Delaglio F, et al. (1995) NMRPipe: A multidimensional spectral processing system based on UNIX pipes. *J Biomol NMR* 6(3):277–293.
46. Jaravine V, Ibraghimov I, Orekhov VY (2006) Removal of a time barrier for high-resolution multidimensional NMR spectroscopy. *Nat Methods* 3(8):605–607.
47. Bartels C, Xia T-H, Billeter M, Güntert P, Wüthrich K (1995) The program XEASY for computer-supported NMR spectral analysis of biological macromolecules. *J Biomol NMR* 6(1):1–10.
48. Kjaergaard M, Poulsen FM (2011) Sequence correction of random coil chemical shifts: Correlation between neighbor correction factors and changes in the Ramachandran distribution. *J Biomol NMR* 50(2):157–165.
49. Sundriyal A, et al. (2014) Inherent regulation of EAL domain-catalyzed hydrolysis of second messenger cyclic di-GMP. *J Biol Chem* 289(10):6978–6990.
50. Kraft D (1994) Algorithm 733: TOMP–Fortran modules for optimal control calculations. *ACM Trans Math Softw* 20(3):262–281.
51. van der Walt S, Colbert SC, Varoquaux G (2011) The NumPy array: A structure for efficient numerical computation. *Comput Sci Eng* 13(2):22–30.
52. Schuck P (2000) Size-distribution analysis of macromolecules by sedimentation velocity ultracentrifugation and lamm equation modeling. *Biophys J* 78(3):1606–1619.
53. Kelly SM, Jess TJ, Price NC (2005) How to study proteins by circular dichroism. *Biochim Biophys Acta* 1751(2):119–139.